Materials Horizons

Design of High Polarization Low Switching Barrier Hybrid Improper Ferroelectric Perovskite Oxide Superlattices

Journal:	*Materials Horizons*
Manuscript ID	MH-COM-08-2023-001285.R1
Article Type:	Communication
Date Submitted by the Author:	09-Oct-2023
Complete List of Authors:	Swamynadhan, M. J.; SRM Institute of Science and Technology, Physics and Nanotechnology; SRM Institute of Science and Technology, Physics and Nanotechnology Ghosh, Ayana; Oak Ridge National Laboratory Computing and Computational Sciences Directorate, Ghosh, Saurabh; SRM Institute of Science and Technology (Deemed to be University), Department of Physics and Nanotechnology

Hybrid improper ferroelectricity (HIF)was discovered in 2011. In this mechanism two primary order parameters couple with the polar mode trilinear and drive the system from paraelectric to ferroelectric phase. In ABO_3-type perovskite oxides with *Pnma* symmetry, rotation (Q_R, $a^0a^0c^+$) and tilt (Q_T, $a^-a^-c^0$) of BO_6 octahedra are the two primary order parameters and with A/A' cation ordering gives rise to ferroelectric polarization. Naturally, it has been believed that functionalities such as polarization can also be switched by tuning these primary order parameters. However, mystery around finding a switching mechanism remains as the polarization switching pathways at finite temperature is unknown. Our study based on density functional theory calculations combined with finite-temperature molecular dynamics simulations shows that the polarization switching follow two different pathways via out of phase rotation and tilt precision, not involving the primary order parameters By considering ABO_3 oxides superlattices, we have established that low polarization switching barrier requires the structure to stay close to cubic symmetry whereas high polarization demands large A-cation mismatch. Thus, "move way" and "close to" cubic symmetry is the key to design high polarization low switching barrier hybrid improper ferroelectrics which can be achieved by tuning the superlattice periodicity.

Journal Name

ARTICLE TYPE

Cite this: DOI: 00.0000/xxxxxxxxxx

Design of High Polarization Low Switching Barrier Hybrid Improper Ferroelectric Perovskite Oxide Superlattices†

M J Swamynadhan,[a] Ayana Ghosh,[b] and Saurabh Ghosh*[a]

Received Date
Accepted Date

DOI: 00.0000/xxxxxxxxxx

Hybrid improper ferroelectricity is a useful tool to design $ABO_3/A'BO_3$ polar superlattices from non polar building blocks. In this study, we have designed high polarization-low switching barrier hybrid improper ferroelectric superlattices with efficient polarization, polarization-magnetization switching properties above room temperature, using density functional theory and *ab initio* molecular dynamics simulations. Superlattices with a chemical formula of $(AAlO_3)_m/(A'AlO_3)_n$, where m/n = 1/1, 1/3, 3/1, 1/5 and 5/1, A, A′ = Lanthanide and Y cations are considered to outline the design principles behind polarization switching and $(LaFeO_3)_3/(CeFeO_3)_1$ is investigated for polarization-magnetization switching. We find that the unconventional switching paths via out-of-phase rotation Q_{R-} ($a^0a^0c^-$) and tilt precession Q_{TP} always yield lower switching barrier compared to those via in-phase rotation Q_{R+} ($a^0a^0c^+$) and tilt Q_T($a^-a^-c^0$) of BO_6 octahedra. Results from *ab initio* molecular dynamics simulations estimate the temperature at which the lowest energy barrier can be overcome. It is possible to tune the polarization switching barrier by tuning tolerance factor, A,A′ cation radius mismatch and super lattice periodicity. For switching via Q_{R-}, the switching barrier varies exponentially with rotation angle, indicating how high switching barrier is expected for systems, away from cubic symmetry. We provide a recipe to overcome such bottleneck by tuning superlattice periodicity. Finally, we have proposed multiferroic device application concept through proposed polarization-temperature hysteresis loop and magnetization switching.

1 Introduction

Designing ferroelectric (FE) materials in which spontaneous polarization couple with other functional properties is one of the key functionalities to be useful in spintronics applications[1–6]. ABO_3-type perovskite oxides are well studied for such multifunctional properties[7–10]. Despite their interesting tri-linear coupling[11,12], most are non-polar in their pristine form[13,14]. The search for ABO_3 perovskite-based FE is still an active area of research. Combining ABO_3 in the form of double/triple perovskites or superlattices with A/A′-site ordering[1,15–19] is one of the proposed measures to achieve ferroelectric ordering by breaking their inversion symmetry. Such symmetry breaking gives rise to spontaneous and switchable polarization resulting from Hybrid improper ferroelectricity (HIF), which is coupled with other functional properties such as magnetization, electronic structure, charge ordering, etc.[20–23]. Figure1 (a)-(d) illustrates how the key structural modes participate in HIF mechanism within *Pnma* symmetry. The trilinear coupling between in-phase rotation Q_{R+} ($a^0a^0c^+$), tilt Q_T ($a^-a^-c^0$) and anti-ferroelectric in-plane A-site displacements Q_{AFE}, F$\sim Q_{R+}\ Q_T\ Q_{AFE}$, drives the system to the lowest symmetry phase. A recent study has reported that the trilinear coupling is also crucial for stabilizing A/A′ cation ordering in oxide double perovskites[24].

In such perovskite-based FE materials with trilinear coupling, polarization (in-plane) switching is possible by tuning either the octahedral rotation or tilt. Hence, multiple switching paths are available with corresponding switching barriers (ΔE). These switching barriers should be small enough for experimental realization and practical applications such as electrocatalysis[25], battery materials[26], photovoltaics[27] and optoelectronics[28]. Interestingly, out-of-phase rotation Q_{R-}($a^0a^0c^-$) and tilt precision Q_{TP} are reported to be the two lowest energy switching pathways, but they do not participate in the trilinear coupling as shown in Figure1(e)[29,30].

The condensation of modes along with stability of a perovskite oxide depend on Goldschmidt tolerance factor τ, as given below

[a] *Department of Physics and Nanotechnology, Faculty of Engineering and Technology, SRM Institute of Science and Technology, Kattankulathur - 603 203, Tamil Nadu, India; E-mail: saurabghosh2802@gmail.com*

[b] *Computational Sciences and Engineering Division, Oak Ridge National Laboratory, Oak Ridge, 37831, TN, USA.*

† Electronic Supplementary Information (ESI) available: [details of any supplementary information available should be included here]. See DOI: 00.0000/00000000.

in Equation 1.

$$\tau = \frac{r_A + r_X}{\sqrt{2}(r_B + r_X)} \quad (1)$$

where r_A, r_B, r_X are the ionic radii of A, B, and X ions respectively. If τ equals 1, the system is in a cubic phase with no rotation or tilt. Both the distortion of BX_6 octahedra and phase transition from cubic to orthorhombic structure arise due to the radius mismatch between A- and B-site cations. It suggests that τ not only decides the stability of the structure but also defines the octahedral rotation and tilt, which is trilinearly coupled with AFE distortion.

Naturally, the ferroelectric phase will be functional below the ferroelectric transition temperature T_c of the system, above which the system becomes para-electric. And previous reports indicate a finite increase in temperature can reduce the coercive voltage of a FE material, which helps to switch the polarization with a lesser external load[31], and can reduce the switching time[32]. Hence, operating temperature is another important parameter in designing FE devices. There are discussions already existing in the literature regarding switching pathways and barrier heights considering HIF super-lattices, but those discussions are based on the density functional theory calculations performed at 0K and do not attend to the questions on the temperature dependence of the switching barriers. A comprehensive cognizance of the switching mechanism detailing the conditions of polarization reversal and how it occurs at finite temperature is still missing[12,21].

In this paper, we have investigated $(AAlO_3)_m/(A'AlO_3)_n$ superlattices (SLs) (where both m and n are odd) with A and A′ cations (A, A′= La, Ce, Nd, Sm, Gd, Dy, Tm, Lu and Y) are arranged in layers along the crystallographic c axis ([001] growth direction) to address the following points listed below:

(a) What are the parameters to tune for the rational design of high polarization low switching barrier (HPLSB) HIF SLs?

(b) How does polarization and magnetization switching happen at finite temperatures?

(c) How temperature dependence of polarization and/or magnetization switching can lead to device concepts?

We have considered $LnAlO_3$ (Ln = Lanthanides and Y) based SLs, due to their diverse τ ranging from ∼1.0 ($LaAlO_3$ - close to cubic) to 0.87 ($LuAlO_3$ - large rotation and tilt). This gives us a large compositional space for τ to play with for predicting HPLSB SLs. We define the τ_{avg} of $(\mathbf{A}AlO_3)_m/(\mathbf{A}'AlO_3)_n$ SL as

$$\tau_{avg} = \frac{m * \tau_A + n * \tau_{A'}}{m+n} \quad (2)$$

Where τ_A and $\tau_{A'}$ are the Goldschmidt tolerance factor of $\mathbf{A}AlO_3$ and $\mathbf{A}'AlO_3$ respectively and m and n are the ratios of the respective layers in SL.

To understand the switching mechanism and the tunability of $\vec{P}$ and ΔE, we first analyze the relation between τ_{avg} and the rotation and tilt of octahedra. It is followed by a detailed study of different conventional, unconventional switching pathways and their corresponding ΔE. We find that unconventional switching paths have lower ΔE than the conventional ones. The most important tuning parameter to design HPLSB SLs is the A, A′ radius mismatch, which tunes both $\vec{P}$ and ΔE. The ratio of A and A′ with (m/n) periodicity in SL is crucial in deciding the barrier height. Within the recipe to design HPLSB SLs, we propose the ambient temperatures for $\vec{P}$ switching utilizing finite temperature *ab initio* molecular dynamics (AIMD) simulations. We show the temperature-dependent hysteresis loop for $\vec{P}$ in $(LaAlO_3)_3/(CeAlO_3)_1$and feasibility of magnetic switching in $(LaFeO_3)_3/(CeFeO_3)_1$ SL through unconventional tilt precession Q_{TP} path, suitable for practical device applications.

2 Computational Details

Density functional theory (DFT)[33] calculations have been performed using the Vienna ab initio simulation package (VASP)[34] within the choice of the projector augmented waves (PAW) basis set[35]. The Perdew-Burke-Ernzerh (PBE) functional has been used to treat the exchange and correlation functional[36]. The cutoff energy is set as 500.0 eV. All the structures have been fully relaxed until all forces on every atom are smaller than 0.001 eV/Å. A dense Γ-centered K-point mesh of 6×6×4 has been used. In the case of MD simulations, the Brillouin zone has been sampled only at the Γ point. Hence we used 2×2×1 super-cell for the MD simulations, and the system is allowed to equilibrate until the distortions and energies are saturated. The canonical ensemble (NVT) by the Nose-Hoover approach[37] has been used[38,39] with a plane wave-basis cut-off energy of 450 eV with 0.5 fs time interval (time steps) between MD steps. We performed a series of MD simulations at different temperatures during the heating and cooling process. At each temperature range, the system is allowed to equilibrate until the distortions and energies are saturated, and the equilibrated structure is considered for further analysis and taken as the initial structure for the next temperature range. The AMPLIMODES (symmetry mode analysis)[40] and PSEUDO[41] (a program for pseudosymmetry search) have been used to understand the structural modes involved in the phase transition.

3 Results and discussion

3.1 Tolerance factor Vs Rotation (Θ_r) and Tilt (Θ_t)

We begin our discussion with the symmetry mode analysis of the SLs. The space group designation of the ground state structure of $(AAlO_3)_1/(A'AlO_3)_3$ SLs is orthorhombic $Pmc2_1$ (space group number 26)[20,42]. There are two symmetry-breaking primary order parameters: (1) in-phase rotation Q_{R+}, ($a^0a^0c^+$) as shown in Figure1(b), (2) out-of-phase tilt Q_T, ($a^-a^-c^0$), as shown in Figure1(c), These primary order parameters couple trilinearly with antiferroelectric (AFE) A-site displacement to stabilize the structure. Interestingly, symmetry breaking of A/A′-site ordering results in non-canceling AFE distortion, which results in net polarization, as shown in Figure1(d)[1,20]. Due to trilinear coupling, $\vec{P}$ direction can be reversed by altering the direction of either in-phase rotation or out-of-phase tilt.

As mentioned earlier in the previous section, τ is an important parameter in deciding the stability of the perovskite structure. In addition, the rotation and tilt angle in ABO_3 perovskites and their derivatives depend on τ. In Figure 2(a), we have shown the variation of 1-τ_{avg} with respect to A and A′cations for $(AAlO_3)_1/(A'AlO_3)_3$ SLs (where, A and A′= La -Lu and Y). here,

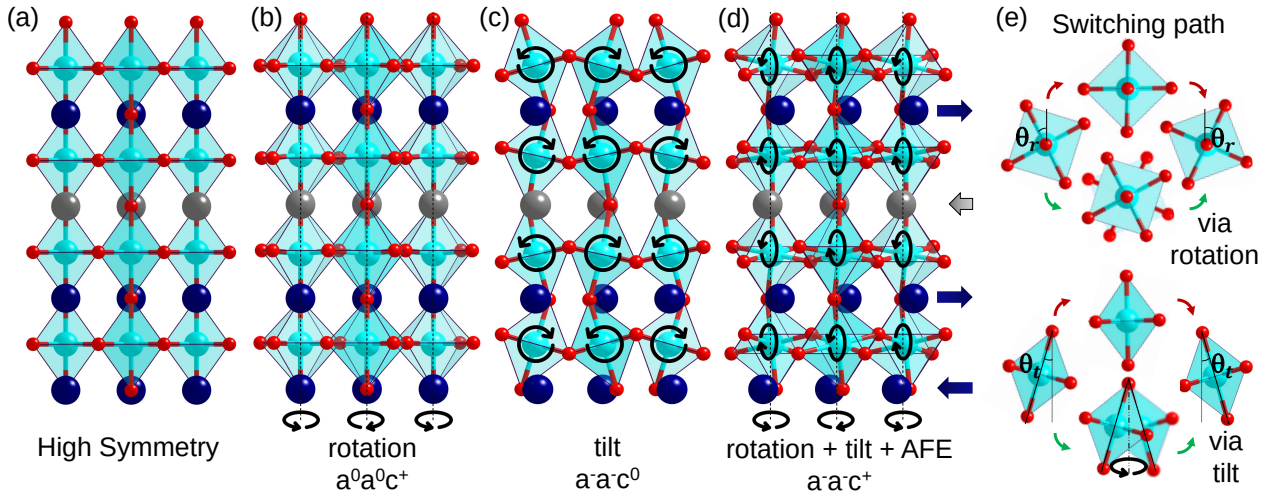

Fig. 1 Trilinear coupling $(AAlO_3)_1/(A'AlO_3)_3$ SLs. (a) 1×3 SL in High Symmetry (b) in-phase rotation ($a^0a^0c^+$) acting on SL (c) out-of-phase tilt ($a^-a^-c^0$) acting on SL (d) non-cancelling in-plane AFE distortion of A and A′ sites as a result of trilinear coupling in 1×3 SL. (e) The conventional (red) and non-conventional (green) switching path for (top) rotation and (bottom) tilt. Here the grey, dark blue, and red atoms indicate A, A′, and oxygen ions, and the cyan color octahedra indicate the BO_6 octahedra. The blue and grey colored arrows are to represent the relative displacement of A and A′ layers.

note that (1-τ_{avg}) measures the deviation from the cubic symmetry. For ideal cubic structure 1-τ_{avg} = 0. For example, considering La and Gd at A and A′ sites, respectively, (1-τ_{avg}) for 3/1 is closer to cubic symmetry than that for 1/3. In Figure 2(b) and (c), we plot the average in-phase rotation angle (θ_r), out-of-phase tilt angle (θ_t) of all SLs considered in this study with respect to $1-\tau_{avg}$. By definition, θ_r and θ_t (Figure1(e)) measure the deviation of the structure from cubic symmetry (θ_r =θ_t=0 for cubic structure). With increase in $1-\tau_{avg}$ (i.e., as τ_{avg} decreases), both θ_r and θ_t linearly increase.[20]

3.2 High Polarization and Low Switching Barrier

Switching paths

Once the linear relationship between $1-\tau_{avg}$ and θ_r, θ_t is established, we continue our discussion on reversal of in-plane $\vec{P}$ direction by tuning θ_r, θ_t via various switching paths. The conventional paths for $\vec{P}$ switching are noted in the following:

(a) Q_{R+} in $P4/mbm$ symmetry where θ_r is zero,

(b) Q_T in *Pmma* symmetry, where θ_t is zero.

The paths are highlighted in red in Figure1(e) in which $+\theta_r$ transitions to $-\theta_r$ via $\theta_r = 0$ or $+\theta_t$ transitions to $-\theta_t$ via $\theta_t = 0$, respectively. For both scenarios, $\vec{P}$ switches from $\vec{P}(+)$ to $\vec{P}(-)$ via $\vec{P} = 0$. The unconventional paths for $\vec{P}$ switching are included below:

(a) θ_r switching via Q_{R-} ($a^0a^0c^-$),

(b) θ_t switching via Q_{TP}, where $\vec{P}$ and tilt are rotated by180° without change in magnitude but direction, i.e from $P_x > 0$ to $P_x < 0$ via $P_y > 0$ or $P_y < 0$, but not via $\vec{P} = 0$. The unconventional paths are shown in Figure1(e), highlighted with green lines. The out-of-phase rotation path Q_{R-} follows a two-step process. First, the odd-numbered layers switch from $+\theta_r$ to $-\theta_r$ via. $\theta_r = 0$, while the even-numbered layers still in their $+\theta_r$ state. In the second step, the even-numbered layers switch from $+\theta_r$ to $-\theta_r$ via. $\theta_r = 0$, while now odd-numbered layers stay in their $-\theta_r$ state. In other words, the rotation switching happens in odd and even-numbered layers at different time steps via an intermediate state with Q_{R-} ($a^0a^0c^-$).

Switching barrier and polarization

We have computed ΔE for various SLs by considering conventional and unconventional switching paths using Nudged Elastic Band (NEB) method as shown in supporting information Figure S1. It becomes evident that the unconventional paths have lower ΔE compared to that of the conventional paths. The reason is that less energy (comparatively) is required to switch two layers than to switch four layers simultaneously. The conventional tilt switching is always higher in energy due to the constrained c lattice parameters, which requires squeezing of octahedra to attain $\theta_t = 0$ state. For all the studied SLs, the energy barriers $\Delta E[\vec{P}(+) \rightarrow \vec{P}(-)]$ are tabulated is Supporting information table S1 which are in the following order:

$\Delta E_{Q_T} > \Delta E_{Q_{R+}} > \Delta E_{Q_{TP}} > \Delta E_{Q_{R-}}$.

Here, ΔE_{Q_T} and $\Delta E_{Q_{R+}}$ are energy barriers for conventional switching pathways via tilt Q_T and in-phase-rotation Q_{R+}, respectively. Whereas, $\Delta E_{Q_{TP}}$ and $\Delta E_{Q_{R-}}$ are energy barriers for unconventional switching pathways via. tilt precision Q_{TP} and out-of-phase rotation Q_{R-}, respectively. The minimum energy barrier is $\Delta E_{Q_{R-}}$, which is plotted as a function of θ_r in Figure 3(a).

There is an exponential increase in $\Delta E_{Q_{R-}}$ with increase in θ_r symbolizing the tunability of $\Delta E_{Q_{R-}}$. Hence, to achieve a low switching barrier, θ_r must be small. We know from our analyses that $1-\tau_{avg}$ should be ideally close to zero to get a small θ_r. There is a misconception that for achieving high polarization, θ_r must be large enough (which also increases the switching barrier). Here, Q_{R+} (measured by θ_r) and Q_T (measured by θ_t) are trillinearly coupled with Q_{AFE}, which will not give net polarization.

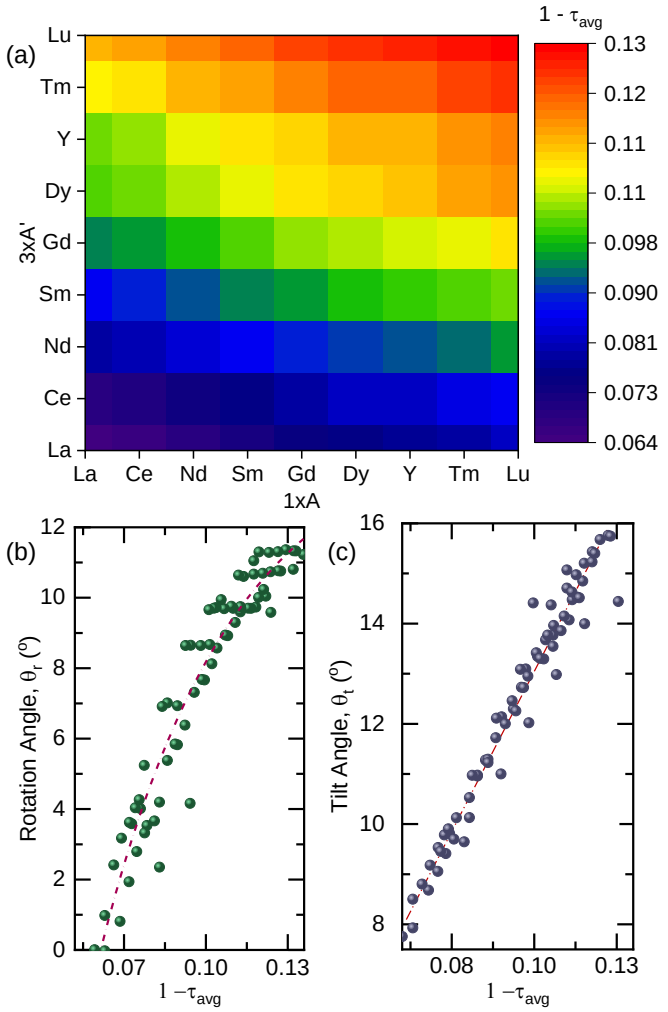

Fig. 2 (a) Heat map of $1-\tau_{avg}$ for all the considered SLs.Here the x-axis and y-axis indicate A and A' sites. At the same time, the heat map color indicates the $1-\tau_{avg}$ of the respective SL. The color bar shows the range of $1-\tau_{avg}$. (b) and (c) The average in-phase rotation angle (θ_r) and the average out-of-phase tilt angle (θ_t) of all the considered SLs against their respective $1-\tau_{avg}$. Here the dotted red lines are for visual aid

$\vec{P}$ arises from the non-canceling displacements of the A and A′-sites from the center of symmetry, which is due to the radius mismatch of A and A′ cations. Figure 3(b) shows $|\vec{P}|$ of $(LaAlO_3)_1/(LuAlO_3)_3$ (i.e, 1/3 SL) and $(LaAlO_3)_3/(LuAlO_3)_1$ (3/1 SL) SL with respect to the normalized polar distortion. The magnitude of $\vec{P}$ is the same for both SLs, $\sim 7\mu C/cm^2$. However, their respective ΔE (Figure 3(b) insets) are quite different. For La/Lu- 3/1 SL, the ΔE is almost half that of La/Lu -1/3 SL. This is due to $\theta_r \sim 0^\circ$ for bulk $LaAlO_3$ and $\theta_r \sim 10^\circ$ for bulk $LuAlO_3$. The ΔE increases with an increase in θ_r, thereby making the barrier for three layers of $LaAlO_3$ less while making it large for three layers of $LuAlO_3$. However, $\vec{P}$ is directly proportional to the relative A-A′ displacement (dl), which depends on the radius mismatch between A and A′ cations ($\Delta r_{(A-A')}$) with only change in the ratio of A and A′ cations. Therefore, $\vec{P}$ does not change much. Figure 3(c) shows the variation of dl with respect to $\Delta r_{(A-A')}$, indicating that for high polarization, $\Delta r_{(A-A')}$ must be large.

Guided by our observations so far, we then consider the $(LaAlO_3)_m/(LnA'O_3)_n$ (where m and n are odd with periods 1/1, 1/3, 1/5, 3/1 and 5/1) SLs for understanding the effect of periodicity on ΔE and $\vec{P}$. Figure-3(d) represents the variation of $\Delta E_{Q_{R-}}$ versus the relative A and A′ displacement dl (as, dl $\propto |P|$) for $(LaAlO_3)_m/(A'AlO_3)_n$ SLs. The plot indicates that the periodicity of the A and A′ layers plays a vital role in tuning the ΔE. For example, if we consider La(1)/Ln(3) SLs (here A′= Ln, Lanthanides and Y) the ΔE are large. There is a rapid increase in barrier height with the increase in $e^{\alpha x}$ where x=dl and α is a coefficient. Interestingly, for Ln(1)/La(5) SLs, ΔE has a comparatively low magnitude compared to the same dl point.

Based on these results, we propose that $\Delta E_{Q_{R-}} \propto e^{\alpha x}$, where $x = dl$ or precisely $\Delta E_{Q_{R-}} \propto e^{\beta|\vec{P}|}$, where β is a parameter dependent on the supercell periodicity. However, a more accurate equation can be derived by performing physics-informed featurization analysis with a large dataset, which does not fall under the scope of our current investigation[24]. Combining these insights, the primary design principles for LPSHB SLs can be outlined as noted below:

(a) both polarization and energy barrier can be tuned by selecting appropriate A, A′ cations, such that the θ_r is small enough to keep ΔE as low as possible, and

(b) large $\Delta r_{A-A'}$ is needed to achieve high polarization. Our results demonstrate how both conditions can be fulfilled by tuning the superlattice periodicity.

3.3 Ambient temperature for Polarization Switching

FE materials have potential applications in nonvolatile ferroelectric random access memory devices (FeRAM), sensors, capacitance, etc.[43]. The efficiency of these ferroelectric devices depends on the $\vec{P}$ switching under external load (voltage or temperature)[32]. Thus, it is important to study the temperature dependence of the $\vec{P}$ switching as the temperature can give sufficient energy for the ferroelectric system to overcome the switching barrier and make the $\vec{P}$(+) and $\vec{P}$(-) states accessible when required. Making the poles accessible has both negative and positive effects[31,32]. An increase in temperature can reduce the coercive voltage of a FE material, which helps to switch the polarization with a lesser external load[31], and can reduce the switching time[32], favorable to fast switching. At the same time, an increase in temperature reduces the polarization in some FE materials[32,44] and favors back-switching[45], which basically reduces the efficiency and storage capability of the FE memory devices[46].

We have studied in-plane $\vec{P}$ switching of the SLs ($(LaAlO_3)_3/(CeAlO_3)_1$) under various temperatures to find the ambient operative temperature suitable for $\vec{P}$ switching by performing AIMD simulations. The initial phase for the AIMD simulation is considered as the system with $\theta_r \sim 0^\circ$ and $P \sim 0\mu C/cm^2$ calculated at 0K. The variation of the θ_r with respect to the system's temperature has been shown in supporting information FigS2. Initially the θ_r increase from $\sim 0^\circ$ and saturates to $\sim 8^\circ$ as the temperature increase from 0K to 100K. Between 100K-300K, the θ_r oscillates around its saturation angle $\sim 8^\circ$. From 300 to 400K, the magnitude of θ_r's oscillation

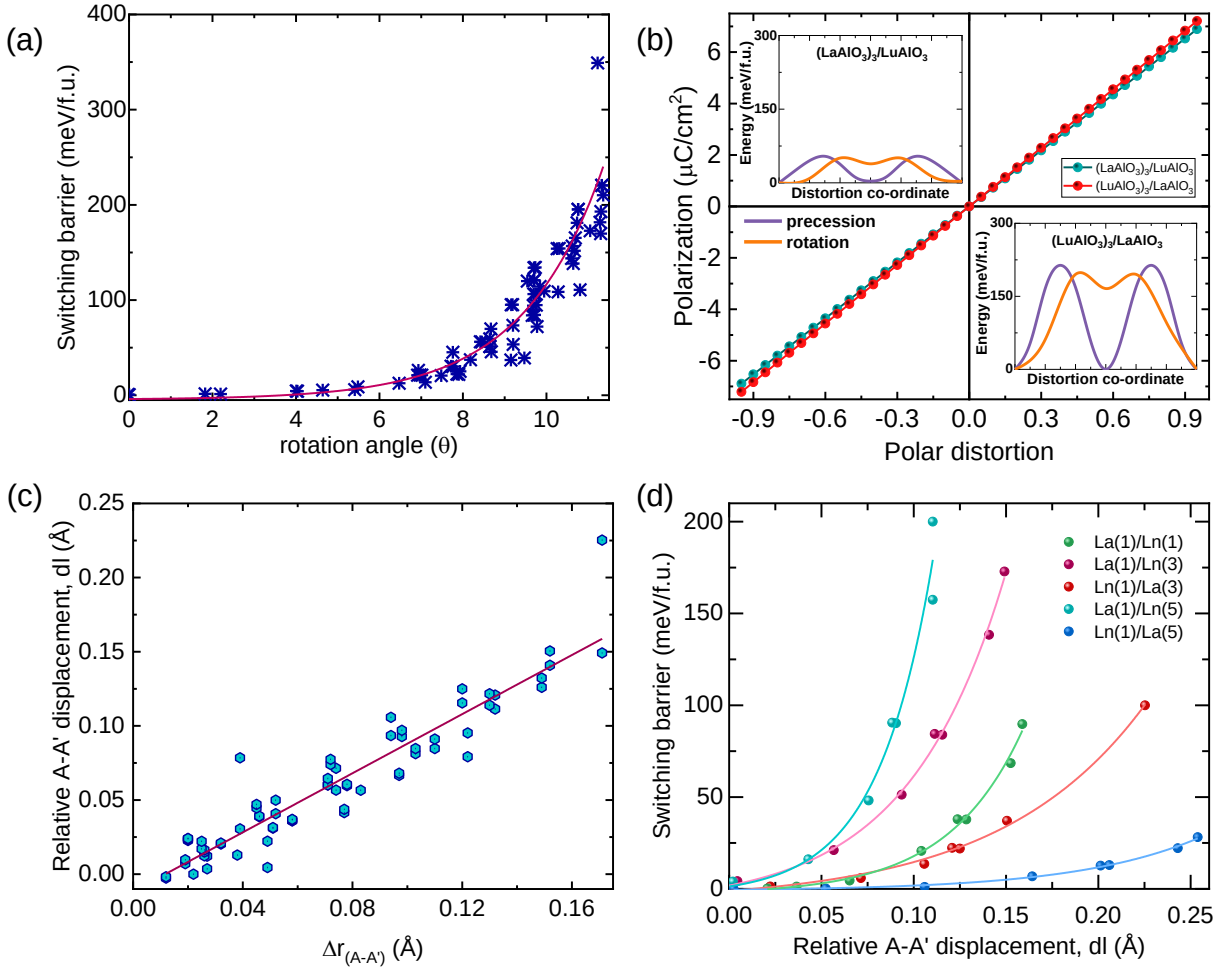

Fig. 3 Tuning parameters and their relations. (a) Energy Barriers of Polarization switching via Out-of-phase rotation Vs the respective rotation angle (θ_r), (b) Comparison of Polarization in $(LaAlO_3)_1/(LuAlO_3)_3$ and $(LuAlO_3)_1/(LaAlO_3)_3$ as a function of normalized polar distortion. The inset figures show the switching barrier for the out-of-phase rotation path and precession path obtained from NEB calculations for the respective systems, (c) Relative displacement of A and A' cations (dl) Vs their ionic radius mismatch ($\Delta r_{(A-A')}$), (d) Switching barrier Vs Relative displacement of A and A' cations (dl) for SLs with different periodicity. Here the solid lines are only for visual guidance.

increases. From 500K onwards, the system attains sufficient energy to cross the ΔE, with accessible $\vec{P}(+)$, $\vec{P}(-)$ states. Hence, we can observe the θ_r switching from positive to negative side back and forth. From 600K, we observe a complete switching of the θ_r from the positive to the negative side. Once the temperature rises further, the fluctuation is rapid, with soaring chances for the system to reach its paraelectric phase. $T > 500K$ provides sufficient energy for the system to cross the ΔE, and the appearance of back-switching or attaining a paraelectric state takes place at a temperature at or above $T > 600K$. Therefore, the ambient switching temperature in the presence of an external field could be between $400 < T < 500K$. Since the switching is aided by both temperature and external field, switching may happen quicker, with a reduced amount of external field, at this temperature range.

The predominant signature of a FE material is in its ability for $\vec{P}$ switching with retention of $\vec{P}$ once the external field is removed. To confirm, we wait for the system to switch itself at 600K, followed by reducing the temperature immediately after $\vec{P}$ switches, as shown in FigS2. Between $500 > T > 300$, the switched θ_r remains negative with fluctuation in magnitude around its saturation angle $\sim -8^\circ$ (the simulation is also extended for a longer period of time for confirmation). Once the temperature is further lowered, the θ_r traces back its initial path (but in the opposite direction), from $\sim -8^\circ$ to $\sim 0^\circ$. Figure 4(a) shows the variation in average θ_r, $|\vec{P}|$ for various temperatures. The shaded regions in red indicate the heating period, while the region in blue represents the cooling period of the simulation. Both θ_r and $\vec{P}$ first increase and then saturates around $\theta_r \sim 8^\circ$, $P \sim 2\mu C/cm^2$ during the heating period. An additional temperature rise reduces θ_r due to constant fluctuation between positive and negative of θ_r. After 600K, the system oscillates rapidly, almost reaching the paraelectric phase with average $\theta_r \sim 0$ and $P \sim 0\mu C/cm^2$. After switching, during the cooling period, the θ_r and P almost follow the same path but in the opposite direction. Together this heating-cooling process of $(LaAlO_3)_3/(CeAlO_3)_1$ shows a temperature dependent hysteresis loop of θ_r and polarization. We have also computed ambient temperatures of $\bar{P}$ (with error bars as indicated) for all

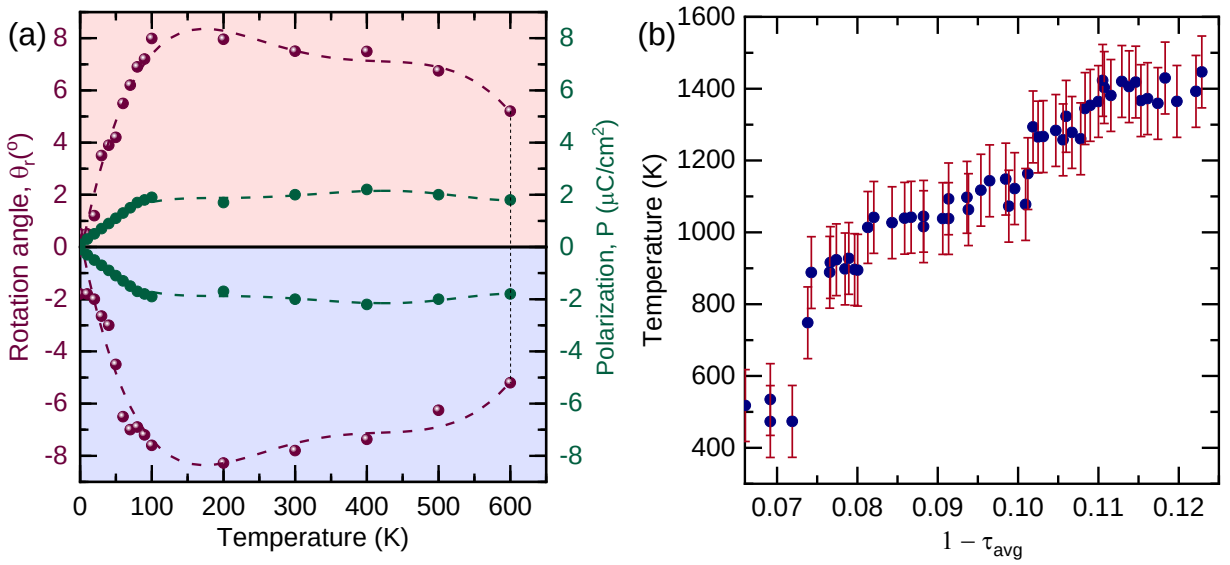

Fig. 4 (a) Temperature dependant Hysteresis loop of polarization in $(LaAlO_3)_3/(CeAlO_3)_1$, here x-axis is the temperature of MD simulation and the y-axis is the average θ_r (red) and net polarization (green) for the respective temperature. Here the red and blue shaded regions represent the heating and cooling phases, respectively. (b) Ambient temperature for the Polarization Vs $1-\tau_{avg}$ of the respective SLs. Here the error bar defines the uncertainty in the temperature.

the considered SLs. Figure 4(b) shows how the ambient temperature increases with increasing $1-\tau_{avg}$. This indicates that being away from the cubic symmetry will increase the switching temperature. However, in such high temperatures, the system is expected to equilibrate to the para-electric phase more rapidly.

3.4 Polarization-Magnetization combined switching

During our AIMD simulations, we have observed that most of the switching happens via. out-pf-phase Q_{R-} rotation. We have also observed tilt switching via precession Q_{TP} in some SLs. Previous reports predict in $(LaFeO_3)/(CeFeO_3)$ 1/1 SL[20] and in $(LaFeO_3)/(BiFeO_3)$ 1/1 SL[47] θ_t switches, then the direction of the canted moment (weak FM) will also switch, resulting in electric-field control of the magnetization. Hence, finally, we consider a magnetic SL $(LaFeO_3)_3/(CeFeO_3)_1$ for multiferroic application. We considered the G-type AFM ordering with the easy axis along x, A-type AFM ordering along the y axis, and an FM canting of spins along the z axis (G_x A_y F_z) as the ground state noncollinear magnetic configuration as reported earlier[48–50]. The ΔE, x and y components of $\vec{P}$ and M_y, M_z components are plotted with respect to precession as shown in Figure 5. We can observe that the polarization goes from $(P_x, P_y) = (-7, 0)$ μC/cm^2 to $(+7, 0)$ μC/cm^2 via $(0, 7)$ μC/cm^2, i.e., the direction of the polarization changes from $-x$ to $+x$ via y, but the magnitude remains constant. During the precession, the out-of-plane weak FM component of magnetization switches from -0.01$\mu_B/f.u.$ to 0.01$\mu_B/f.u.$ which is shown in Figure 5(b), which show the switching of weak FM when the tilt switches via precession, which could be further studied for multiferroic applications.

To observe this polarization-magnetic switching, we performed AIMD simulation in this $(LaFeO_3)_3/(CeFeO_3)_1$ system at 1200K

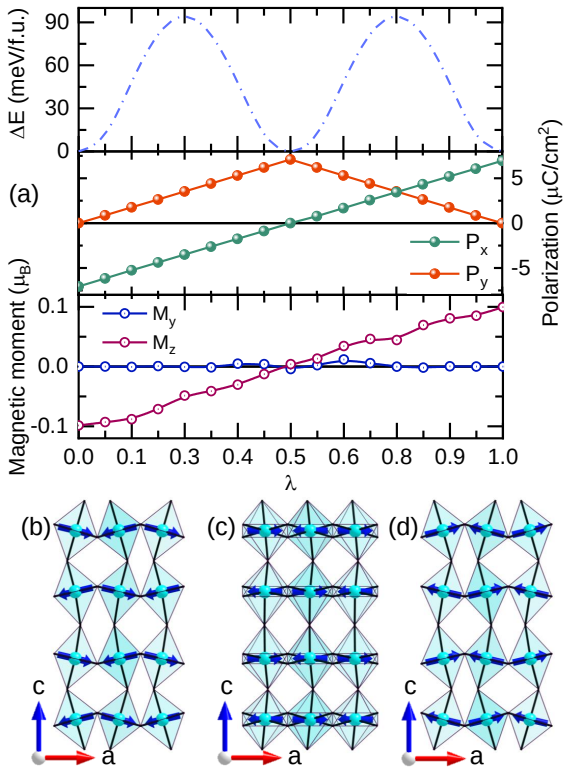

Fig. 5 Magnetization switching in $(LaFeO_3)_3/(CeFeO_3)_1$. (a) (top) The energy barrier for precession from $+P_x$ to $-P_x$ in meV per formula unit, (middle) P_x (red) and P_y (green) polarization components, (bottom) M_y (blue) and M_z (pink) magnetization components as a function of normalized distortion (precession). (b) Schematic explaining the precession process and shows the direction of magnetic spins before (left), during (middle), and after (right) the polarization switching.

(much above the ambient temperature) to observe the polarization switching via Q_{R-} and Q_{TP}. Since the simulation temperature is much above the ambient temperature, we observed multiple switching, and most of the switching occurred via Q_{R-} and few via Q_{TP}. Whenever the Polarization switches via Q_{TP}, the weak FM component of magnetization changes its direction. The tilt switching with magnetization switching from AIMD plots are shown in supporting information Figure S3, which is similar to the magnetization switching shown in Figure 5

4 Conclusions

Our first-principles study on a series of SLs identifies design principles behind designing SLs with high polarization and low switching barriers. Our analyses have shown strong interdependence between the τ_{avg} or $1-\tau_{avg}$, rotation (θ_r), and tilt angles (θ_t) of the octahedra which become the key tunable parameters for tuning barrier heights. The most common/favorable switching paths are the unconventional ones via out-of-phase rotation and tilt precession which differs from the current understanding of feasible switching paths. The additional tuning parameters are A-A' radius mismatch and the supercell periodicity. Interestingly, it is possible to tune the barrier height with no drastic change in polarization just by tuning the periodicity. The polarization switching is temperature-dependent. The ambient temperature for switching has a strong relationship with $1-\tau_{avg}$. The temperature-dependent hysteresis loop of polarization and complementary switching magnetization further enhance these SLs' suitability in device applications.

Conflicts of interest

There are no conflicts to declare.

Acknowledgements

S.G. and M.J.S. sincerely acknowledge the funding support from DST-National Supercomputing Mission, File. No. DST/NSM/R&D_HPC_Applications/2021/34. The authors sincerely acknowledge SRMIST HPCC and IISC Banglore Parampravega for providing computational resources. This research (A.G.) was sponsored by the Laboratory Directed Research and Development Program of Oak Ridge National Laboratory, managed by UT-Battelle, LLC, for the U. S. Department of Energy. ORNL is managed by UT-Battelle, LLC, for DOE under Contract No. DE-AC05-00OR22725.

Notes and references

1 A. T. Mulder, N. A. Benedek, J. M. Rondinelli and C. J. Fennie, *Advanced Functional Materials*, 2013, **23**, 4810–4820.

2 L. W. Martin and D. G. Schlom, *Current Opinion in Solid State and Materials Science*, 2012, **16**, 199–215.

3 I. H. Lone, J. Aslam, N. R. Radwan, A. H. Bashal, A. F. Ajlouni and A. Akhter, *Nanoscale research letters*, 2019, **14**, 1–12.

4 B. Sun, G. Zhou, L. Sun, H. Zhao, Y. Chen, F. Yang, Y. Zhao and Q. Song, *Nanoscale Horizons*, 2021, **6**, 939–970.

5 A. Popkov, M. Davydova, K. Zvezdin, S. Solov'Yov and A. Zvezdin, *Physical Review B*, 2016, **93**, 094435.

6 L. Weston, X. Cui, S. P. Ringer and C. Stampfl, *Physical Review B*, 2016, **93**, 165210.

7 J. Geusic, S. Kurtz, L. Van Uitert and S. Wemple, *Applied Physics Letters*, 1964, **4**, 141–143.

8 M. DiDomenico Jr and S. Wemple, *Physical Review*, 1968, **166**, 565.

9 S. M. Selbach, T. Tybell, M.-A. Einarsrud and T. Grande, *Advanced materials*, 2008, **20**, 3692–3696.

10 J. Wang, J. Neaton, H. Zheng, V. Nagarajan, S. Ogale, B. Liu, D. Viehland, V. Vaithyanathan, D. Schlom, U. Waghmare *et al.*, *science*, 2003, **299**, 1719–1722.

11 P. Ghosez and J.-M. Triscone, *Nature Materials*, 2011, **10**, 269–270.

12 N. A. Benedek, A. T. Mulder and C. J. Fennie, *Journal of Solid State Chemistry*, 2012, **195**, 11–20.

13 K. Patel, S. Prosandeev, Y. Yang, B. Xu, J. Íñiguez and L. Bellaiche, *Physical Review B*, 2016, **94**, 054107.

14 R. S. Roth, *J. Res. Natl. Bur. Stand*, 1957, **58**, 75.

15 H. Wang, F. Tang, M. Stengel, H. Xiang, Q. An, T. Low and X. Wu, *Physical review letters*, 2022, **128**, 197601.

16 J. M. Rondinelli and C. J. Fennie, *Advanced Materials*, 2012, **24**, 1961–1968.

17 M. Saliba, T. Matsui, J.-Y. Seo, K. Domanski, J.-P. Correa-Baena, M. K. Nazeeruddin, S. M. Zakeeruddin, W. Tress, A. Abate, A. Hagfeldt *et al.*, *Energy & environmental science*, 2016, **9**, 1989–1997.

18 H. Asano, J. Hayakawa and M. Matsui, *Applied physics letters*, 1997, **71**, 844–846.

19 T. Fukushima, A. Stroppa, S. Picozzi and J. M. Perez-Mato, *Physical Chemistry Chemical Physics*, 2011, **13**, 12186–12190.

20 M. Shaikh, M. Karmakar and S. Ghosh, *Physical Review B*, 2020, **101**, 054101.

21 N. A. Benedek and M. A. Hayward, *Annual Review of Materials Research*, 2022, **52**, 331–355.

22 A. Stroppa, P. Barone, P. Jain, J. M. Perez-Mato and S. Picozzi, *Advanced Materials*, 2013, **25**, 2284–2290.

23 Y. S. Oh, X. Luo, F.-T. Huang, Y. Wang and S.-W. Cheong, *Nature materials*, 2015, **14**, 407–413.

24 A. Ghosh, G. Palanichamy, D. P. Trujillo, M. Shaikh and S. Ghosh, *Chemistry of Materials*, 2022, **34**, 7563–7578.

25 J. Hwang, R. R. Rao, L. Giordano, Y. Katayama, Y. Yu and Y. Shao-Horn, *Science*, 2017, **358**, 751–756.

26 T. Yi, W. Chen, L. Cheng, R. D. Bayliss, F. Lin, M. R. Plews, D. Nordlund, M. M. Doeff, K. A. Persson and J. Cabana, *Chemistry of Materials*, 2017, **29**, 1561–1568.

27 J.-P. Correa-Baena, M. Saliba, T. Buonassisi, M. Grätzel, A. Abate, W. Tress and A. Hagfeldt, *Science*, 2017, **358**, 739–744.

28 M. V. Kovalenko, L. Protesescu and M. I. Bodnarchuk, *Science*, 2017, **358**, 745–750.

29 L. Wang, W. Pan, D. Han, W. Hu and D. Sun, *Physical Chemistry Chemical Physics*, 2020, **22**, 5826–5831.

30 J. Varignon, N. C. Bristowe, E. Bousquet and P. Ghosez, *Scientific reports*, 2015, **5**, 15364.

31 H. Chen, L. Tang, L. Liu, Y. Chen, H. Luo, X. Yuan and D. Zhang, *Materialia*, 2020, **14**, 100919.

32 Y. Zhang, X. Zhong, Z. Chen, J. Wang and Y. Zhou, *Journal of Applied Physics*, 2011, **110**, 014102.

33 P. Hohenberg and W. Kohn, *Phys. Rev. B*, 1964, **136**, 864.

34 G. Kresse and J. Furthmüller, 1996.

35 P. E. Blöchl, *Physical review B*, 1994, **50**, 17953.

36 J. P. Perdew, K. Burke and M. Ernzerhof, *Phys. Rev. Lett.*, 1996, **77**, 3865–3868.

37 S. Nosé, *The Journal of chemical physics*, 1984, **81**, 511–519.

38 G. Kresse and J. Hafner, *Physical Review B*, 1993, **48**, 13115.

39 G. Kresse and J. Hafner, *Physical Review B*, 1994, **49**, 14251.

40 E. Kroumova, M. Aroyo, J. Perez-Mato, S. Ivantchev, J. Igartua and H. Wondratschek, *Journal of applied crystallography*, 2001, **34**, 783–784.

41 A. K. Kirov, M. I. Aroyo and J. M. Perez-Mato, *Journal of applied crystallography*, 2003, **36**, 1085–1089.

42 H. Sim, S. Cheong and B. G. Kim, *Physical review B*, 2013, **88**, 014101.

43 J. Scott, *science*, 2007, **315**, 954–959.

44 A. Jiang and T. Tang, *Journal of Applied Physics*, 2008, **104**, 024104.

45 A. Picinin, M. Lente, J. Eiras and J. Rino, *Physical Review B*, 2004, **69**, 064117.

46 D. Fu, K. Suzuki, K. Kato and H. Suzuki, *Applied physics letters*, 2003, **82**, 2130–2132.

47 Z. Zanolli, J. C. Wojdeł, J. Íniguez and P. Ghosez, *Physical Review B*, 2013, **88**, 060102.

48 M. Robbins, G. Wertheim, A. Menth and R. Sherwood, *Journal of Physics and Chemistry of Solids*, 1969, **30**, 1823–1825.

49 H. J. Zhao, W. Ren, Y. Yang, X. M. Chen and L. Bellaiche, *Journal of Physics: Condensed Matter*, 2013, **25**, 466002.

50 L. Bellaiche, Z. Gui and I. A. Kornev, *Journal of Physics: Condensed Matter*, 2012, **24**, 312201.